Published in final edited form as:
Free Radic Biol Med. 2011 February 1; 50(3): 459–468. doi:10.1016/j.freeradbiomed.2010.11.028.

Magnetic resonance imaging of organic contrast agents in mice: capturing the whole-body redox landscape

Ryan M. Davis[1], **Shingo Matsumoto**[1], **Marcelino Bernardo**[2,3], **Anastasia Sowers**[1], **Ken-Ichiro Matsumoto**[4], **Murali C. Krishna**[1], and **James B. Mitchell**[1]

[1]Radiation Biology Branch, Center for Cancer Research, National Cancer Institute, Bethesda, Maryland 20892

[2]Molecular Imaging Program, NCI, NIH.

[3]SAIC-Frederick, NCI-Frederick, Frederick, MD, USA.

[4]Molecular Imaging Center, National Institute of Radiological Sciences, Chiba, Japan.

Abstract

Nitroxides are a class of stable free radicals that have several biomedical applications including radioprotection and non-invasive assessment of tissue redox status. For both of these applications, it is necessary to understand the *in vivo* biodistribution and reduction of nitroxides. In this study, magnetic resonance imaging was used to compare tissue accumulation (concentration) and reduction of two commonly studied nitroxides: the piperidine nitroxide Tempol and the pyrrolidine nitroxide 3-CP. It was found that 3-CP is reduced three to eleven times slower (depending on the tissue) than Tempol *in vivo*, and that maximum tissue concentration varies substantially between tissues (0.6 mM – 7.2 mM.) For a given tissue, the maximum concentration usually did not vary between the two nitroxides. Furthermore, using electron paramagnetic resonance (EPR) spectroscopy, it was shown that the nitroxide reduction rate depends only weakly on cellular pO_2 in the oxygen range expected *in vivo*. These observations, taken with the marked variation in nitroxide reduction rates observed between tissues, suggest that tissue pO_2 is not a major determinant of the nitroxide reduction rate *in vivo*. For the purpose of redox imaging, 3-CP was shown to be an optimal choice based on the achievable concentrations and bioreduction observed *in vivo*.

Keywords

Magnetic resonance imaging (MRI); nitroxides; redox; radioprotection; electron paramagnetic resonance spectroscopy

Introduction

Redox magnetic resonance imaging is a technique that uses T_1 contrast from paramagnetic nitroxide free radicals (also called aminoxyl radicals) to monitor the intracellular redox

Address Correspondence to: Ryan Davis, Radiation Biology Branch, National Cancer Institute, Bldg. 10, Room B3-B69, 9000 Rockville Pike, Bethesda, MD 20892, Phone: (301) 402-9013, Fax: (301) 480-2238, davisrm2@mail.nih.gov.

status of tissues [1]. The redox status of tissue is influenced by several biochemical factors such as the degree of reduction of the ubiquinol pool in mitochondria [2–3]; NADH dehydrogenase activity [2]; the local tissue oxygen concentration [4]; the activity of pentose phosphate enzymes [5]; and the levels of endogenous antioxidants such as ascorbate [6], glutathione [4], NADH, and NADPH [7]. Disease states or pathological conditions including sepsis [8], stroke, inflammation, ischemia-reperfusion injury [9], and cancer [10–12] are associated with oxidative stress or altered metabolism, which may modulate or correlate with the redox status of cells. Therefore, it may be useful in a research or clinical setting to monitor the redox status of tissue. Nitroxides are low molecular weight (~200 Da) MRI contrast agents that, when injected *in vivo*, interact with various enzymes and reducing equivalents. In addition to their SOD mimic activity [13–15] and stimulation of catalase-like activity of hemeproteins [16], nitroxides also intercept intracellular reducing species, and thus participate in various oxidation-reduction (redox) reactions [17–18]. Through these reactions, an equilibrium is established between the nitroxide and its reduced counterpart, the non-contrast enhancing hydroxylamine; this equilibrium greatly favors the hydroxylamine. The aggregate of these reactions results in an overall exponential decay in tissue nitroxide levels with time, which occurs at a rate that is strongly influenced by the level of intracellular reducing species [1]. Thus, monitoring nitroxide reduction *in vivo* provides a non-invasive means to monitor intracellular tissue redox status.

Nitroxide-based redox imaging was initiated with electron paramagnetic resonance imaging (EPRI), which directly measures the unpaired electron on the nitroxide [19–21]. Due to the relatively low spatial resolution of EPRI and its inability to provide anatomical images, redox imaging was limited to larger and more easily localized tissues such as superficial tumors and leg muscle [4,21]. In response to these limitations, it was hypothesized that T_1 shortening properties of nitroxides would allow high resolution monitoring of nitroxide dynamics, while simultaneously providing high-resolution anatomical images for reference. Subsequent studies found that MRI was capable of measuring nitroxide reduction rates with high accuracy (compared to EPRI) [22], and was capable of monitoring nitroxide reduction with sub-millimeter resolution in small animal models of cancer [23]. Thus, MRI enables redox imaging with resolution not feasible with EPRI [24–26], greatly increasing potential applications.

Published studies using nitroxide-based MRI redox imaging have focused primarily on tumor, muscle, kidney [25], salivary glands [26], and brain [24]. These studies have established that the rate of nitroxide reduction varies significantly between different nitroxides, with 3-CP reducing much more slowly than Tempol [25]. In the current study, the redox status (nitroxide reduction rates) and nitroxide concentration is reported for 3-CP and Tempol in an expanded number of tissues. Nitroxide uptake and reduction rates were found to vary widely among tissues and different tumors, and in agreement with previous studies [24–26], 3-CP reduced much more slowly than Tempol. The results reported here suggest that 3-CP provided reliable redox measurements for the imaging conditions used in this study.

Methods

Chemicals

Tempol (4-hydroxy-2,2,6,6-tetramethylpiperidine-1-oxyl; TP) and (3-carbomyl-2,2,5,5-tetramethyl-1-pyrrolidine-1-oxyl; 3-CP) were purchased from Sigma-Aldrich (St. Louis, MO, USA.)

Animal Studies

Female C3HHenCrMTV- and athymic nude mice were obtained from the Frederick Cancer Research Center, Animal Production (Frederick, MD, USA). Mice were housed in a climate controlled circadian rhythm adjusted room, and were allowed access to food and water *ad libidum*. The body weight of the mice at the time of imaging was 22–30 grams. Tumor cells were injected into the subcutaneous space of the right hind leg. Squamous cell carcinoma (SCCVII) cells ($2–3 \times 10^5$) or KHT cells ($4–5 \times 10^5$) were injected 7–10 days before imaging in C3H mice while human colon carcinoma cells (HT-29) cells (10^6) were injected 14 days before imaging in nude mice. Tumor size was approximately 1 cm^3 at the time of imaging. All experiments were carried out in compliance with the Guide for the Care and Use of Laboratory Animal Resources (National Research Council, 1996) and approved by the National Cancer Institute Animal Care and Use Committee.

Imaging Protocol

Both tumor bearing and non-tumor bearing mice were anesthetized with a mixture of isofluorane (4% to induce, 1–2% to maintain) and medical air (750 mL/min). A catheter was made by breaking the tip off of a 30½ gauge needle (Becton Dickinson and Company, Franklin Lakes, NJ) and inserting it into Tygon tubing (inner diameter (id): 0.01 inches, Norton Performance Plastics, Akron, Ohio.) This catheter was placed in a tail vein and connected to a syringe containing either Tempol (5μL/g body weight of 150mM Tempol in PBS) or 3-CP (5μL/g body weight of 150mM 3-CP in PBS), with an injection volume of 115–150 μL depending on the weight of the mouse. The mouse was then placed inside the MRI coil in a prone position, and lightly taped to the cradle once at the head, once just above the hind legs, and once on the tail. The syringe was placed outside of the scanner so that it could be accessed during imaging. The surface body temperature was maintained between 35°C and 36°C, and the breathing rate was maintained between 60–90 breaths per min.

Images were acquired on a 3T Phillips clinical scanner with a custom-built small animal receive-only saddle-shaped coil (diameter: 3.8 cm, length 7.0 cm.) After localizing scans, a multi-slice T_2 weighted turbo spin echo (TSE) (TR = 4s, TE = 30ms, α=90°, NEX =1, FOV = 8×3.96 cm, slice thickness = 1 mm, number of slices = 22) was acquired to aid in identification of tissue boundaries. Then, a 3D spoiled fast field echo (FFE) (TR = 8.5 ms, TE = 2.302 ms (fat and water in phase), α=3°, NEX = 3, FOV = 8×3.4cm, slice thickness = 1mm, number of slices = 22) was acquired for T_1 map calculation (described below.) For the dynamic scans, a 3D spoiled fast field echo (FFE) at a higher FA (α=19°, NEX = 1, time per scan = 20 seconds, number of dynamic scans was 60 for Tempol and 60 or 120 for 3-CP, depending on the target tissues). After 2 min of baseline imaging, the nitroxide was manually injected starting at the beginning of the seventh image. Imaging resumed for 18 min in the case of Tempol and 18 or 38 min in the case of 3-CP. Once the scanning was complete, the animal was allowed to recover from anesthesia, and was then returned to its cage.

In vivo calculation of nitroxide concentration

The calculation of nitroxide concentration was performed on a voxel by voxel basis using Matlab (The MathWorks, Inc., Natick, MA, USA), and is based on the initial (pre enhancement) longitudinal recovery time ($T_{1,0}$) of voxel, the relaxivity of the nitroxide, and the fast field echo signal equation. To calculate initial T_1 maps, the ratio of signal in a low flip angle (α = 3°, TR = 8.5 ms, NEX = 3, TE = 2.302 ms) and high flip angle (α = 19°, TR = 8.5 ms, NEX = 3, TE = 2.302 ms) fast field echo image was calculated. The FFE signal equation was used to create a lookup table that relates the ratio of signals of the high and low flip angle image to the T_1 of the voxel. The FFE equation is:

$$S(T_{t,1},\alpha,T_R)=A\sin(\alpha)\left(\frac{1-e^{-\frac{T_R}{T_{1,t}}}}{1-\cos(\alpha)e^{-\frac{T_R}{T_{1,t}}}}\right) \quad (1)$$

where α is the flip angle in degrees, T_R is the repetition time in seconds, $T_{1,t}$ is the longitudinal recovery time at time *t*, and A accounts for proton density and T_2 relaxation. In general, the ratio between high and low flip angle image intensity increases as the T_1 decreases. Using the lookup table, T_1 maps of the tissue were generated on a voxel by voxel basis.

Once the T_1 map was calculated, the concentration in each voxel at each time point was calculated from the relaxivity of the nitroxide, the T_1 of the voxel, and the percent signal enhancement of the voxel. Nitroxides create signal enhancement by shortening the T_1 of surrounding water protons:

$$\frac{1}{T_{1,t}}-\frac{1}{T_{1,0}}=r_1[N] \quad (2)$$

where r_1 is the longitudinal relaxivity of the contrast agent (0.20 $mM^{-1}s^{-1}$ for both Tempol and 3-CP), $T_{1,t}$ is the longitudinal recovery time at time *t*, and [N] is the concentration of nitroxide in mM. Substituting equation 2 into equation 1, and dividing by the signal at t = 0, allows calculation of percent signal enhancement as a function of nitroxide concentration in the voxel, and the $T_{1,0}$ and flip angle of the voxel:

$$\frac{S_t}{S_0}=f(T_{1,0},r_1,\alpha,[N]) \quad (3)$$

Numerically solving the above equation for [N] shows that for a given T_1,r_1, and α, the percent signal enhancement (S_t/S_0) monotonically increases as the concentration increases. This relationship is inverted and least squares fit with a third order polynomial:

$$[N]=a(T_{1,0},r_1,\alpha)\left(\frac{S_t}{S_0}\right)^3+b(T_{1,0},r_1,\alpha)\left(\frac{S_t}{S_0}\right)^2+c(T_{1,0},r_1,\alpha)\left(\frac{S_t}{S_0}\right)^1+d(T_{1,0},r_1,\alpha) \quad (4)$$

So that a, b, c, and d are tabulated for a range (0.3s – 3s) of $T_{1,0}$ values. For each image slice of each time point, the nitroxide concentration is calculated from the percent signal enhancement on a voxel by voxel basis (S_t/S_0) using the above equation.

Calculation of tissue concentrations

To measure the concentration of nitroxide in a tissue, the concentration over the entire image was calculated on a voxel by voxel basis as described above. Then, in each image slice that contained the tissue of interest, regions of interest (ROI) were manually drawn around the tissue (Figure 1). Finally, the average tissue concentration was calculated by averaging the voxel by voxel concentration throughout the multi-slice ROI.

Calculation of relaxivity

Blood was extracted from the hearts of sacrificed mice and immediately deposited into lithium heparin tubes (Starstedt AG & Co, Nümbrecht, Germany.) To oxidize any reducing agents that might be in the blood, 3% hydrogen peroxide and 50mM copper sulfate were mixed into the blood in final concentrations of 5 mM and 50 μM, respectively. Next, Tempol or 3-CP was mixed into blood or phosphate buffered saline at 10 mM, 7.5 mM, 5 mM, and 2.5 mM and imaged at room temperature.

The relaxivity measurements were performed by using an inversion recovery turbo-spin echo sequence (IR-TSE) to measure the T_1 of the vials. Regions of interest were drawn over each vial, and the average signal (S) in the region was fit with a three parameter model:

$$S(TI)=\left|S_{inf}\left[1-(1-k)\cdot e^{-\frac{TI}{T_1}}\right]\right| \tag{5}$$

where S_{inf} is the signal of the vial at equilibrium, k is the cosine of the flip angle of the inversion recovery sequence, and T_1 is the longitudinal recovery time of the blood in the vial. Using this method, the T_1 was calculated for each vial, and the value of $1/T_1$ (in s^{-1}) was plotted as a function of the vial concentration (in mM). The slope of the $1/T_1$ vs. concentration plot is the relaxivity (in $s^{-1}mM^{-1}$) of the nitroxide in blood at room temperature. A linear least squares fit was used to determine the slope.

Calculation of In Vivo reduction rate

Using the GraphPad Prism 5.03 curve fitting toolbox, a mono- or bi-exponential model (depending on the tissue) was fit to the average tissue concentration time-courses from 3–8 animals. The model equations are

$$[N(t)]=ae^{-krt}+b, \tag{6}$$

$$[N(t)]=ae^{-k_r t}+ce^{-l_r t} \tag{7}$$

Where *a*, *b*, and *c* are in mM, and k_r is the reduction rate in min^{-1}. Statistical comparisons of reduction rates between tissues were performed with the extra-sum-of-squares F test (GraphPad.) For tissues fit with a bi-exponential model, a separate statistical test was performed for each exponential component.

Measurement of nitroxide reduction in cell suspensions with EPR

Electron paramagnetic resonance (EPR) was used to measure the reduction of nitroxides in cell suspensions under varying pO_2 conditions. A heated oxygen/CO_2/nitrogen gas mixture was blown through the resonator to maintain the air temperature at 37 ± 0.2 °C. Gas mixtures (Roberts Oxygen Co., Inc., Rockville, Maryland) contained different oxygen concentrations of 0 mmHg, 7.6×10^{-4} mmHg, 0.76 mmHg, 7.6 mmHg, 30.4 mmHg, or 152 mm Hg, each with 5% CO_2 and the balance nitrogen. Before measuring cellular reduction of the nitroxide, a standard Tempol sample (100μM) was placed in the resonator. The scan range was set to zero mG, and the microwave frequency was set so that it coincided with peak absorption, and was kept constant throughout the experiment. SCCVII cells were grown in RPMI 1640 medium supplemented with 10% fetal calf serum and antibiotics. Exponentially growing cells (monolayer) were trypsinized, counted, and re-suspended at 10^8

cells/ml in RPMI medium in a 1.5 mL Eppendorf tube (Hamburg, Germany) and maintained at 37°C. Tempol or 3-CP was mixed into the cell suspension to create a 100 μM solution. The solution was vortexed, and then drawn into a gas permeable tube, which was then placed into the EPR resonator. Finally, the sample was scanned over 15 min as the cells metabolized the nitroxide. After the scan was finished, the natural logarithm of the signal minus baseline was plotted versus time. From the slope of the resulting line, the nitroxide reduction decay constant was derived. Due to systematic (non-oxygen dependent) variations in nitroxide reduction rates on different experiment days, a paired T-test was used to test the significance of the reduction rate on oxygen dependence. The anoxic reading was paired with the ambient air reading of the same day.

Results

Figure 2 displays representative images of the dynamic uptake and reduction of Tempol and 3-CP. A coronal image from a typical Tempol (Figure 2a) and 3-CP (Figure 2b) experiment is shown, with the submandibular salivary gland and tongue outlined. As can be seen, both Tempol and 3-CP rapidly accumulated throughout the mouse's head after injection. As time progresses, the concentration of nitroxide in the head decreased toward zero. When the average ROI concentration is plotted in a graph (Figure 2c), the nitroxide concentration underwent exponential decay as a function of time. Comparing both the graphs and the reduction rates (k_r values in the legend of Figure 2c) of each curve shows that the rate of nitroxide reduction varies between different tissues and different nitroxides. An alternate way to visualize redox status is by calculating a "reduction map", where the entire redox time-course is summarized by a single image (Figure 2d and Figure 2e). Reduction rate maps are obtained by first spatially smoothing the raw images with a square averaging filter (11×11×1 voxels, 1.7×1.7×1 mm.) Then, the time-concentration curve for each voxel is fit with an exponential decay model, and the decay rate of the fit is assigned to the corresponding voxel in the reduction map. Examples of redox maps are shown in Figure 2d for Tempol and Figure 2e for 3-CP. It is seen that in the tongue and the surrounding muscle the reduction rate is fairly homogeneous, while in the salivary gland the reduction rate appears heterogeneous.

Nitroxide reduction in non-cancerous tissues

From the dynamic MRI imaging experiments, Tempol and 3-CP concentrations were calculated as a function of time in the jugular vein, and in eight non-cancerous normal tissues (Figure 3). The exponential decay rates in each tissue were calculated from these experiments and the results are tabulated in Table 1. Tempol was reduced the slowest in leg muscle ($0.51 \pm 0.35\ min^{-1}$) and the fastest in the salivary glands ($2.3 \pm 0.15\ min^{-1}$.) 3-CP was also reduced the slowest in leg muscle ($0.038 \pm 0.035\ min^{-1}$) but reduced the fastest in the lacrimal gland ($1.9 \pm 0.4\ min^{-1}$.) The blood concentration (an ROI was drawn inside the jugular vein) for 3-CP appeared to be bi-exponential, while for Tempol the blood concentration appeared mono-exponential. It was found that for the salivary gland, rectum, lacrimal glands, brain, and liver the reduction rate of Tempol was not significantly different from the rate of blood clearance. This was in contrast with 3-CP, where the tissue reduction rates were significantly different from the venous clearance rate.

Several tissues were localized in which nitroxide reduction measurements were not possible. Factors such as organ motion, motion artifacts due to breathing, sub-resolution organ size, and no apparent nitroxide uptake contributed to the inability of MRI to measure nitroxide reduction in these tissues (Table 2).

Nitroxide reduction in tumor tissues

The reduction rate of Tempol was measured *in vivo* for SCCVII, HT-29, and KHT tumor lines (Table 3). Tempol reduction varied between tumor lines, and exhibited the following order: HT-29 < KHT < SCC. The reduction rate of each of these tissues was significantly different from muscle and the SCCVII tumor line. In SCCVII tumors, Tempol was reduced approximately 10 times faster than 3-CP.

Dependence of nitroxide reduction rate on oxygen concentration

Under hypoxic conditions, many nitroxides tend to be reduced more quickly than under normoxic conditions [3–4,27]. The degree to which reduction changes between hypoxic and normoxic conditions varies markedly between nitroxides and cell types [3,27]. To measure the dependence of the nitroxide reduction rate on oxygen concentration (pO_2), the reduction rates of 3-CP and Tempol were measured in a suspension of SCCVII cells using EPR spectrometry. The pO_2 was maintained at 0, 7.6×10^{-4}, 0.76, 7.6, 30.4, or 152 mmHg over the course of each experiment. Figure 4 shows the reduction rate of Tempol and 3-CP as a function of pO_2. For both nitroxides, the reduction rate increased as the pO_2 was decreased. For Tempol, the reduction rate (k_r) at 0 mmHg was 80% faster than at 152 mmHg ($P(k_{r,0\ mmHg} > k_{r,152\ mmHg}) = 0.026$). For 3-CP, the reduction rate at 0 mmHg was 140% faster than at 152 mmHg ($P(k_{r,0\ mmHg} > k_{r,152\ mmHg}) = 0.03$.) The large error bars reflect systematic (non-oxygen dependent) differences in nitroxide reduction between different experiment days. On average, the reduction rate of Tempol in SCCIV cells was approximately 6 times faster than the reduction rate of 3-CP for all oxygen concentrations. These results are in agreement with prior studies that suggest that nitroxides are reduced more rapidly under hypoxic conditions than under ambient air conditions [3–4,27]. Thus, varying levels of hypoxia may contribute to the differing *in vivo* reduction rates observed in different tumor lines (Table 3).

Nitroxide Tissue Dose

Because Tempol and 3-CP have concentration-dependent biological effects which include antioxidant activity, hypertensive effects, and radioprotection, the nitroxide concentration was quantified as a function of time after injection. The maximum tissue concentrations and the time to reach maximum are shown in Table 4. The maximum blood concentration for Tempol was 8.1 ± 1.3 mM for Tempol and was 6.6 ± 2.0 mM for 3-CP, and this difference was not statistically significant. For both nitroxides, the maximum concentration was the lowest in the muscle (3-CP: 0.8 ± 0.1 mM, Tempol: 0.6 ± 0.1 mM), while the maximum concentration was the highest in the kidney (Tempol: 7.2 ± 0.5 mM, 3-CP: 6.1 ± 0.8 mM.) Tumors received less nitroxide than all tissues except for muscle (and brain for 3-CP.) In most tissues, the maximum concentration was not significantly different between the nitroxides.

Tempol administered *in vivo* was found to be at higher concentrations in healthy tissues than in tumor tissues (Table 4). This differential concentration may account for the selective radioprotection that is observed in murine cancer models [26,28]. To test the duration of differential concentration, the concentration of nitroxide in healthy tissues minus the concentration in SCCVII tissues was plotted as a function of time (Figure 5). It was found in the case of Tempol that the liver, rectum, salivary gland, tongue, and leg muscle all contained greater concentrations of nitroxide than the tumor for approximately two minutes post-injection (Figure 5a). In the case of 3-CP, it was found that the liver, rectum, and salivary gland each contained more nitroxide than the tumor for 3–4 minutes after injection (Figure 5b).

Error in reduction rate parameter

The estimation accuracy of the nitroxide reduction rate is limited by factors including the signal enhancement to noise ratio and the rate at which the nitroxides reduce. Thus, the 95% confidence interval was tabulated for both nitroxides in various tissues (Table 5). It was found that with the exception of the tongue, the slowly reducing nitroxide 3-CP allows estimation of the reduction rate with greater statistical certainty than Tempol.

Discussion

Until recently, the relatively low spatial resolution and lack of anatomical images provided by EPR imaging restricted redox imaging to large and easily localizable tissues such as muscle and tumor. The results of the present study show that it is possible to overcome these limitations using MRI, which allowed determination of Tempol and 3-CP reduction rates in an expanded number organs, each with different reduction and uptake levels (Figures 1, 3, 4 and Tables 1 & 3). These results suggest that redox MRI is capable of monitoring local disease or therapy induced redox changes in a variety of distinct tissues. Although MRI expands the tissues accessible to redox imaging, nitroxide reduction could not be monitored in some tissues due to low nitroxide uptake or organ size and motion (Table 2). In future studies, respiratory gating or stronger encoding gradients may help to overcome these limiting effects.

Nitroxides, in addition to being redox-sensitive imaging probes, exhibit several biological effects, including *in vivo* radioprotection. In general, a clinical radioprotector, when administered before radiation therapy, can reduce adverse side effects in healthy tissues, while leaving the tumor unaffected. Currently, the most commonly used clinical radioprotector is amifostine, which effectively reduces healthy tissue damage during radiation therapy of head and neck squamous cell carcinoma, non small cell lung cancer, and pelvic malignancies [29–30]. However, amifostine has non-lethal and transient side effects including hypotension, vomiting, and allergic reactions [31]. Furthermore, there is uncertainty as to whether or not amifostine protects tumors [30,32–33], which would reduce the therapeutic gain of treatment. Both the success of amifostine in protecting healthy tissues as well as the controversy surrounding possible radioprotection of tumors has spurred a search for other radioprotectors to further improve outcome during radiation therapy [34].

Nitroxides have long been known to provide both *in vitro* and *in vivo* radioprotection [28,35–36], and the level of radioprotection is believed to increase when higher concentrations of the nitroxide are present at the time of radiation exposure [36]. Furthermore, the nitroxide Tempol, much like amifostine, protects against radiation-induced reduction in saliva flow in mouse xerostomia models [26,37]. Unlike amifostine, however, nitroxides have the rare capability of enabling non-invasive tissue detection because of their MRI signal enhancing properties (Figure 3). Using this capability, we have shown that both Tempol and 3-CP have two properties that suggest they may preferentially protect healthy tissues over tumor tissue. First, the peak concentration of Tempol is greater in many healthy tissues than in SCC, KHT, and HT-29 tumor lines (Table 4). Second, the nitroxide radical accumulated to higher concentrations in healthy tissues than in SCC tumor for 0–4 minutes after injection (Figure 5). A fair criticism of nitroxides as radioprotectors is that their bioreduction makes the therapeutic window for radioprotection quite narrow, and therefore not practical for clinical use. Therefore, in order to make nitroxides clinically practical radioprotectors, they must reduce much more slowly in human tissues than in the murine tissues studied here.

In the context of radioprotection, there are two possible ways to overcome the limitations of rapid nitroxide reduction. The first is that it may be possible to synthesize a radioprotecting

nitroxide that reduces much more slowly than the nitroxides studied here. As suggested by the findings of this study (Figure 5), this may result in differential nitroxide concentration for periods longer than a few minutes. Another way that the limitation of rapid nitroxide reduction may be overcome is due to inherent differences in reduction rates between humans and mice. In all mammals, antioxidants such as NADH and $FADH_2$ are required during oxygen metabolism. Because the rate of oxygen metabolism is 5–30 times greater in mice than in humans [38–39], it may be the case that murine tissues contain higher levels metabolic antioxidants. In addition, metabolic antioxidants are coupled to antioxidant pools such as NADPH and glutathione [40], which may also be involved in nitroxide reduction [4,7]. If murine cells were equipped with higher levels of antioxidants to compensate for relatively rapid rates of oxygen metabolism, it would be expected that murine tissues would reduce nitroxides much more quickly than human tissues. Thus, nitroxide reduction rates may be inherently slower in humans than in mice. Fortunately, if nitroxides are ever used as radioprotectors in humans, nitroxide reduction could easily be assessed with MRI.

One aim of this study was to determine which nitroxide is optimal for imaging at 3 Tesla, a field strength typical of clinical scanners. This study suggests that 3-CP is the optimal nitroxide for at least two reasons. The first reason is that in most tissues, the calculated reduction rate for 3-CP has smaller 95% confidence intervals than does Tempol (Table 4). The smaller confidence intervals of 3-CP are mostly due to its slower reduction rate, which provides more samples per reduction rate calculation. More samples per experiment partially compensates for noise in the measurements, which has the effect of decreasing the confidence interval width. Thus, the benefit of a slowly reducing nitroxide depends on the signal enhancement to noise ratio, which varies between different scanners or imaging sequences. For example, field strengths higher than 3T may have a higher signal enhancement to noise ratio, which may make the confidence intervals of Tempol comparable to those of 3-CP. In that case, Tempol would be the preferable contrast agent because it requires a shorter scan time.

The second reason why 3-CP may be preferable to Tempol for redox imaging is because in some tissues the reduction rate of Tempol is not significantly different from the arterial clearance rate (Table 1). This may be a problem, because an assumption of the reduction rate calculation is that signal change through time is predominantly due to nitroxide reduction. In the case when the apparent tissue reduction rate is comparable to or greater than the rate at which the nitroxide accumulates into the tissue, factors such as intravascular enhancement and nitroxide extravasation will also affect the MRI signal change. Thus, for the case of the salivary gland, lacrimal gland, brain, rectum, and liver, it is not clear if input from the artery to the tissue affects the apparent reduction rate. Use of 3-CP as a redox imaging contrast agent apparently overcomes this effect, because all tissues except for the lacrimal gland and kidney reduced 3-CP significantly more slowly than the rate of arterial clearance.

Previous studies have reported reduction rates in selected tissues, these studies are in moderate agreement with the present findings. Reports of 3-CP reduction in muscle vary from $0.037\ min^{-1} \pm 0.005$ [41] to $0.067 \pm 0.0108\ min^{-1}$ [23], which is similar to the value of $0.06 \pm 0.03\ min^{-1}$ reported here. Two reports measured the reduction rate of 3-CP in SCC tumors as $0.0973 \pm 0.009\ min^{-1}$ [23] and $0.107 \pm 0.020\ min^{-1}$ [25], which are consistent with the values of $0.11 \pm 0.01\ min^{-1}$ reported here. Finally, Hyodo et al published tissue reduction rates of Tempol and 3-CP for blood, SCC(VII) tumor, muscle, and kidney that were 5–30% lower than the values reported here [25]. Although the tissue reduction rates presented here are in relative agreement with the findings of other studies, the reduction rate of Tempol in the salivary gland presented here is markedly larger than in a previous study [26]. The size and location of ROI selection in the salivary gland did not substantially affect the calculated reduction rate of Tempol in the salivary gland (data not shown.) In the

previous study [26], SCCVII or HT-29 tumors were implanted in the front leg as opposed to the hind leg as was done in the present study, and this may account for differences in the redox status and/or blood flow in the nearby salivary gland. In general, the studies summarized here are consistent with our findings that Tempol reduces 3 (liver) to 11 (SCC) times faster than 3-CP *in vivo*, and that tumor tissue reduces nitroxides faster than muscle, but slower than all other measured tissues.

The rate of nitroxide reduction was found to vary among tumor types (Table 2). Because nitroxides can be reduced to the hydroxylamine indirectly by transition metals and reactive oxygen species, or directly by a reducing agent, both the levels of reactive oxygen species as well as the redox status of intracellular redox pairs may alter nitroxide reduction rates [42]. In particular, since oxygen is the ultimate electron acceptor for redox molecules in the mitochondria, and because these redox molecules reduce Tempol [2], tissue oxygenation may modulate the rate of nitroxide reduction [3,43–44]. To test if there is an effect of oxygen on nitroxide reduction in SCCVII cells, *in vitro* experiments were performed where the reduction rate of 3-CP and Tempol were determined as a function of oxygen concentration. These experiments suggest that the degree of cellular oxygenation plays a role in the rate of nitroxide reduction in cells (Figure 4). The oxygen dependence of the reduction rate may be due to several factors. First, as stated above, oxygen functions as an electron acceptor for intracellular redox reactions, so that an adequate supply of oxygen will cause the intracellular environment to become relatively oxidized, causing nitroxide reduction to proceed more slowly. Second, increased tissue oxygenation may increase the rate at which the hydroxylamine is oxidized to the nitroxide [3], causing the apparent reduction rate to decrease. Both of these explanations are consistent with the observation that 3-CP metabolism slows when tumor bearing mice breathe carbogen [4]. Therefore, variations in tumor oxygenation may partly account for the differences in Tempol reduction observed between tumor types.

The degree to which oxygen influences the rate of nitroxide reduction has been studied by other investigators for a variety of nitroxides and tissues. In general, the dependence of nitroxide reduction on cellular oxygenation status varied markedly between nitroxides and cell types. For example, in TB cells, the lipophillic nitroxide 5-Doxyl stearate was reduced approximately 15 times faster when the cells were exposed to anoxic conditions rather than ambient air [3,27]. In contrast, the same cells exhibited only a two fold increase in reduction rate for the water soluble nitroxide 3-CP (Figure 4 in this study, reference [27]). In the case of Tempol, the results from this study and other studies suggest that the oxygen dependence of reduction is cell-type dependent. In mammalian TB cells [27], and rat hepatocytes [43], no significant oxygen dependence of Tempol reduction was observed. In contrast, this study showed a significant dependence of the rate of Tempol reduction on oxygen concentration in SCC(VII) cells (Figure 4). This suggests that the degree of oxygen dependence on nitroxide reduction may vary between cell types. Indeed, other nitroxides such as PCA and Tempamine show an oxygen dependence that varies between cell types [27,43]. The causes of variations in the oxygen dependence may be due to differences in nitroxide compartmentalization and/or inherent redox differences between cells. Taken together, the *in vitro* and *in vivo* studies reviewed here are in agreement with the *in vitro* findings of the current study, where a two-fold increase in the nitroxide reduction rate was observed under anoxic conditions.

This study suggests that variations in tissue pO_2 are not solely responsible for the range of reduction rates observed between tissues. This claim is supported by comparing the variations in reduction rates between tissues (Table 1) to the variations in reduction rates for different oxygen concentrations (Figure 4). In this study, variations in nitroxide reduction rates between healthy tissues were as large as 4 for Tempol and 7 for 3-CP. These variations

are much greater than the factor of 2 change observed between ambient and hypoxic conditions in cancer cells *in vitro*. Furthermore, it is expected that most non-cancerous tissues are more oxygenated than cancerous tissues, so that if oxygen were the only factor, the net reduction of nitroxides may be slower in non-cancerous tissues than in cancerous tissues. Thus, it is likely that effects not directly related to oxygen also play a substantial role in the reduction of nitroxides. This is consistent with the observation that cytosolic enzymes and antioxidants such as G6PD [5], ascorbate [6], glutathione [4], NADH, and NADPH [7] are involved in nitroxide reduction. Lastly, faster tumor nitroxide reduction might also be influenced by elevated steady-state levels of superoxide reported in occur in tumors where SOD activity is lower than in normal tissues [45].

Conclusion

MRI is capable of mapping redox status and nitroxide dose in at least eight distinct murine tissues, while simultaneously providing anatomical images for registration. This capability may greatly increase the potential applications of redox imaging, allowing monitoring of redox changes during disease onset and progression. The findings of this study suggest that 3-CP is superior to Tempol for redox imaging. In terms of radioprotection, it was found that nitroxides accumulate in non-cancerous tissues at greater concentrations than in tumor, suggesting that nitroxides may selectively protect healthy tissues over cancer tissues. In conclusion, MRI is an effective method for measuring nitroxide dynamics and may expand the potential applications of redox imaging.

Acknowledgments

We would like to thank Dr. Pete Choyke for his provision of imaging resources. We would like to thank Dr. Brenda Klaunberg for her assistance in identifying murine tissues on MR images.

This research was supported by the Intramural Research Program of the Center for Cancer Research, National Cancer Institute, NIH.

List of Abbreviations

EPR	electron paramagnetic resonance
EPRI	electron paramagnetic resonance imaging
k_r	reduction rate
pO_2	partial oxygen pressure
SCC	Squamous Cell Carcinoma
Tpl	Tempol

References

1. Hyodo F, Soule BP, Matsumoto K, Matusmoto S, Cook JA, Hyodo E, Sowers AL, Krishna MC, Mitchell JB. Assessment of tissue redox status using metabolic responsive contrast agents and magnetic resonance imaging. J Pharm Pharmacol 2008;60:1049–1060. [PubMed: 18644197]
2. Trnka J, Blaikie FH, Smith RA, Murphy MP. A mitochondria-targeted nitroxide is reduced to its hydroxylamine by ubiquinol in mitochondria. Free Radic Biol Med 2008;44:1406–1419. [PubMed: 18206669]
3. Chen K, Glockner JF, Morse PD 2nd, Swartz HM. Effects of oxygen on the metabolism of nitroxide spin labels in cells. Biochemistry 1989;28:2496–2501. [PubMed: 2543442]

4. Ilangovan G, Li SH, Zweier JL, Krishna MC, Mitchell JB, Kuppusamy P. In vivo measurement of regional oxygenation and imaging of redox status in RIF-1 murine tumor: effect of carbogen-breathing. Magn Reson Med 2002;48:723–730. [PubMed: 12353291]
5. Samuni Y, Gamson J, Samuni A, Yamada K, Russo A, Krishna MC, Mitchell JB. Factors influencing nitroxide reduction and cytotoxicity in vitro. Antioxid Redox Signal 2004;6:587–595. [PubMed: 15130285]
6. Couet WR, Brasch RC, Sosnovsky G, Tozer TN. Factors affecting nitroxide reduction in ascorbate solution and tissue homogenates. Magn Reson Imaging 1985;3:83–88. [PubMed: 3999940]
7. Fuchs J, Mehlhorn RJ, Packer L. Free radical reduction mechanisms in mouse epidermis skin homogenates. J Invest Dermatol 1989;93:633–640. [PubMed: 2551971]
8. von Dessauer B, Bongain J, Molina V, Quilodran J, Castillo R, Rodrigo R. Oxidative stress as a novel target in pediatric sepsis management. J Crit Care. 2010
9. Cuzzocrea S, Riley DP, Caputi AP, Salvemini D. Antioxidant therapy: a new pharmacological approach in shock, inflammation, and ischemia/reperfusion injury. Pharmacol Rev 2001;53:135–159. [PubMed: 11171943]
10. Szatrowski TP, Nathan CF. Production of large amounts of hydrogen peroxide by human tumor cells. Cancer Res 1991;51:794–798. [PubMed: 1846317]
11. Xia C, Meng Q, Liu LZ, Rojanasakul Y, Wang XR, Jiang BH. Reactive oxygen species regulate angiogenesis and tumor growth through vascular endothelial growth factor. Cancer Res 2007;67:10823–10830. [PubMed: 18006827]
12. Yamaura M, Mitsushita J, Furuta S, Kiniwa Y, Ashida A, Goto Y, Shang WH, Kubodera M, Kato M, Takata M, Saida T, Kamata T. NADPH oxidase 4 contributes to transformation phenotype of melanoma cells by regulating G2-M cell cycle progression. Cancer Res 2009;69:2647–2654. [PubMed: 19276355]
13. Samuni A, Krishna CM, Riesz P, Finkelstein E, Russo A. A novel metal-free low molecular weight superoxide dismutase mimic. J Biol Chem 1988;263:17921–17924. [PubMed: 2848018]
14. Krishna MC, Grahame DA, Samuni A, Mitchell JB, Russo A. Oxoammonium cation intermediate in the nitroxide-catalyzed dismutation of superoxide. Proc Natl Acad Sci U S A 1992;89:5537–5541. [PubMed: 1319064]
15. Krishna MC, Russo A, Mitchell JB, Goldstein S, Dafni H, Samuni A. Do nitroxide antioxidants act as scavengers of O2-. or as SOD mimics? J Biol Chem 1996;271:26026–26031. [PubMed: 8824242]
16. Krishna MC, Samuni A, Taira J, Goldstein S, Mitchell JB, Russo A. Stimulation by nitroxides of catalase-like activity of hemeproteins. Kinetics and mechanism. J Biol Chem 1996;271:26018–26025. [PubMed: 8824241]
17. Swartz HM, Sentjurc M, Morse PD 2nd. Cellular metabolism of water-soluble nitroxides: effect on rate of reduction of cell/nitroxide ratio, oxygen concentrations and permeability of nitroxides. Biochim Biophys Acta 1986;888:82–90. [PubMed: 3741890]
18. Samuni AM, DeGraff W, Krishna MC, Mitchell JB. Cellular sites of H2O2-induced damage and their protection by nitroxides. Biochim Biophys Acta 2001;1525:70–76. [PubMed: 11342255]
19. Kuppusamy P, Shankar RA, Zweier JL. In vivo measurement of arterial and venous oxygenation in the rat using 3D spectral-spatial electron paramagnetic resonance imaging. Phys Med Biol 1998;43:1837–1844. [PubMed: 9703045]
20. Ilangovan G, Li H, Zweier JL, Kuppusamy P. In vivo measurement of tumor redox environment using EPR spectroscopy. Mol Cell Biochem 2002;234–235:393–398.
21. Kuppusamy P, Afeworki M, Shankar RA, Coffin D, Krishna MC, Hahn SM, Mitchell JB, Zweier JL. In vivo electron paramagnetic resonance imaging of tumor heterogeneity and oxygenation in a murine model. Cancer Res 1998;58:1562–1568. [PubMed: 9537265]
22. Hyodo F, Murugesan R, Matsumoto K, Hyodo E, Subramanian S, Mitchell JB, Krishna MC. Monitoring redox-sensitive paramagnetic contrast agent by EPRI, OMRI and MRI. J Magn Reson 2008;190:105–112. [PubMed: 18006345]
23. Matsumoto K, Hyodo F, Matsumoto A, Koretsky AP, Sowers AL, Mitchell JB, Krishna MC. High-resolution mapping of tumor redox status by magnetic resonance imaging using nitroxides as redox-sensitive contrast agents. Clin Cancer Res 2006;12:2455–2462. [PubMed: 16638852]

24. Hyodo F, Chuang KH, Goloshevsky AG, Sulima A, Griffiths GL, Mitchell JB, Koretsky AP, Krishna MC. Brain redox imaging using blood-brain barrier-permeable nitroxide MRI contrast agent. J Cereb Blood Flow Metab 2008;28:1165–1174. [PubMed: 18270519]
25. Hyodo F, Matsumoto K, Matsumoto A, Mitchell JB, Krishna MC. Probing the intracellular redox status of tumors with magnetic resonance imaging and redox-sensitive contrast agents. Cancer Res 2006;66:9921–9928. [PubMed: 17047054]
26. Cotrim AP, Hyodo F, Matsumoto K, Sowers AL, Cook JA, Baum BJ, Krishna MC, Mitchell JB. Differential radiation protection of salivary glands versus tumor by Tempol with accompanying tissue assessment of Tempol by magnetic resonance imaging. Clin Cancer Res 2007;13:4928–4933. [PubMed: 17699873]
27. Swartz HM, Chen K, Pals M, Sentjurc M, Morse PD 2nd. Hypoxia-sensitive NMR contrast agents. Magn Reson Med 1986;3:169–174. [PubMed: 3959885]
28. Hahn SM, Sullivan FJ, DeLuca AM, Krishna CM, Wersto N, Venzon D, Russo A, Mitchell JB. Evaluation of tempol radioprotection in a murine tumor model. Free Radic Biol Med 1997;22:1211–1216. [PubMed: 9098095]
29. Winczura P, Jassem J. Combined treatment with cytoprotective agents and radiotherapy. Cancer Treat Rev 2010;36:268–275. [PubMed: 20044209]
30. Sasse AD, Clark LG, Sasse EC, Clark OA. Amifostine reduces side effects and improves complete response rate during radiotherapy: results of a meta-analysis. Int J Radiat Oncol Biol Phys 2006;64:784–791. [PubMed: 16198504]
31. Rades D, Fehlauer F, Bajrovic A, Mahlmann B, Richter E, Alberti W. Serious adverse effects of amifostine during radiotherapy in head and neck cancer patients. Radiother Oncol 2004;70:261–264. [PubMed: 15064010]
32. Brizel DM, Overgaard J. Does amifostine have a role in chemoradiation treatment? Lancet Oncol 2003;4:378–381. [PubMed: 12788413]
33. Lindegaard JC, Grau C. Has the outlook improved for amifostine as a clinical radioprotector? Radiother Oncol 2000;57:113–118. [PubMed: 11054513]
34. Greenberger JS. Radioprotection. In Vivo 2009;23:323–336. [PubMed: 19414422]
35. Hahn SM, Tochner Z, Krishna CM, Glass J, Wilson L, Samuni A, Sprague M, Venzon D, Glatstein E, Mitchell JB, et al. Tempol, a stable free radical, is a novel murine radiation protector. Cancer Res 1992;52:1750–1753. [PubMed: 1551104]
36. Mitchell JB, DeGraff W, Kaufman D, Krishna MC, Samuni A, Finkelstein E, Ahn MS, Hahn SM, Gamson J, Russo A. Inhibition of oxygen-dependent radiation-induced damage by the nitroxide superoxide dismutase mimic, tempol. Arch Biochem Biophys 1991;289:62–70. [PubMed: 1654848]
37. Vitolo JM, Cotrim AP, Sowers AL, Russo A, Wellner RB, Pillemer SR, Mitchell JB, Baum BJ. The stable nitroxide tempol facilitates salivary gland protection during head and neck irradiation in a mouse model. Clin Cancer Res 2004;10:1807–1812. [PubMed: 15014035]
38. Elliott KA. Metabolism of brain tissue slices and suspensions from various mammals. J Neurophysiol 1948;11:473–484. [PubMed: 18894652]
39. Tolmasoff JM, Ono T, Cutler RG. Superoxide dismutase: correlation with life-span and specific metabolic rate in primate species. Proc Natl Acad Sci U S A 1980;77:2777–2781. [PubMed: 6771758]
40. Mitchell JB, Russo A. The role of glutathione in radiation and drug induced cytotoxicity. Br J Cancer Suppl 1987;8:96–104. [PubMed: 3307879]
41. Kuppusamy P, Li H, Ilangovan G, Cardounel AJ, Zweier JL, Yamada K, Krishna MC, Mitchell JB. Noninvasive imaging of tumor redox status and its modification by tissue glutathione levels. Cancer Res 2002;62:307–312. [PubMed: 11782393]
42. Soule BP, Hyodo F, Matsumoto K, Simone NL, Cook JA, Krishna MC, Mitchell JB. The chemistry and biology of nitroxide compounds. Free Radic Biol Med 2007;42:1632–1650. [PubMed: 17462532]
43. Iannone A, Hu HP, Tomasi A, Vannini V, Swartz HM. Metabolism of aqueous soluble nitroxides in hepatocytes: effects of cell integrity, oxygen, and structure of nitroxides. Biochim Biophys Acta 1989;991:90–96. [PubMed: 2540844]

44. Swartz HM, Chen K, Hu HP, Hideg K. Contrast agents for magnetic resonance spectroscopy: a method to obtain increased information in in vivo and in vitro spectroscopy. Magn Reson Med 1991;22:372–377. discussion 378. [PubMed: 1812373]

45. Oberley LW, Buettner GR. Role of superoxide dismutase in cancer: a review. Cancer Res 1979;39:1141–1149. [PubMed: 217531]

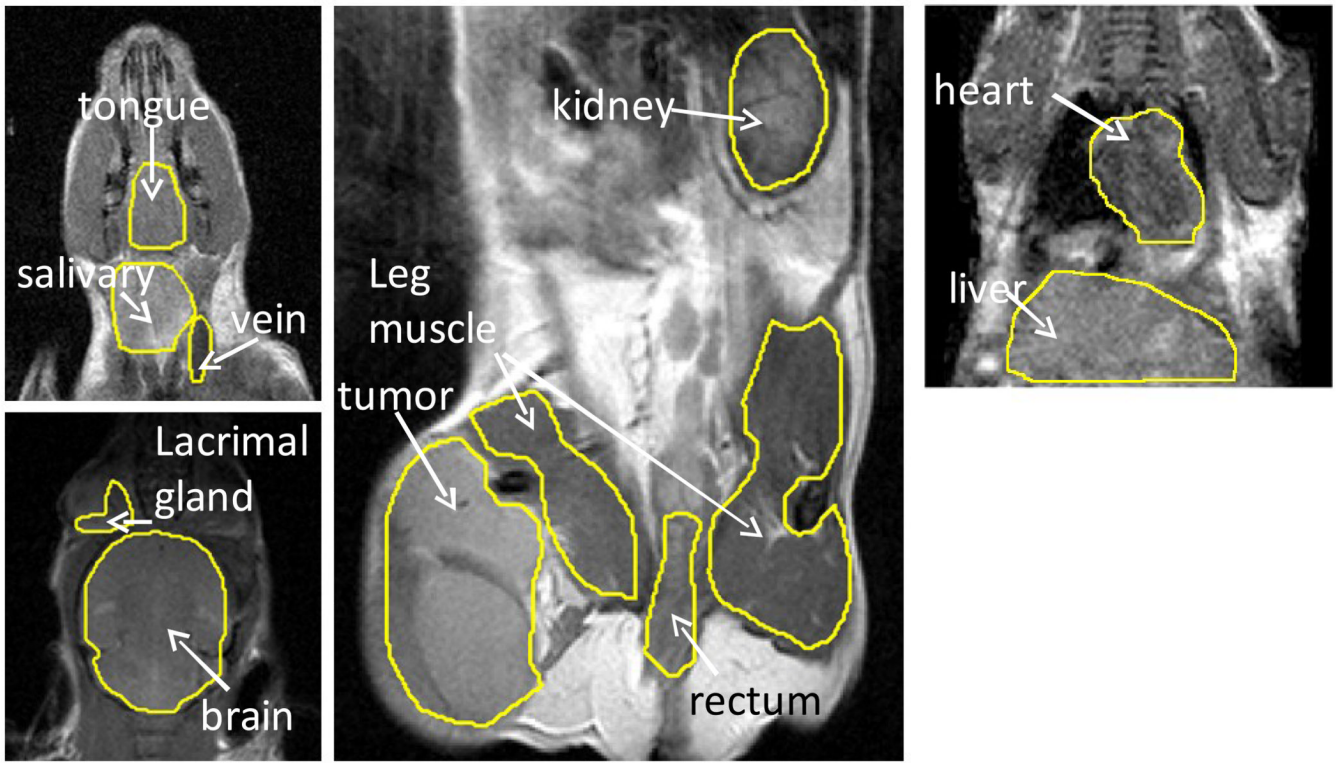

Figure 1.
T_2 weighted MRI images showing the tissues studied in this work. Abbreviations: vein: jugular vein; salivary: submandibular salivary gland; SCC: squamous cell carcinoma.

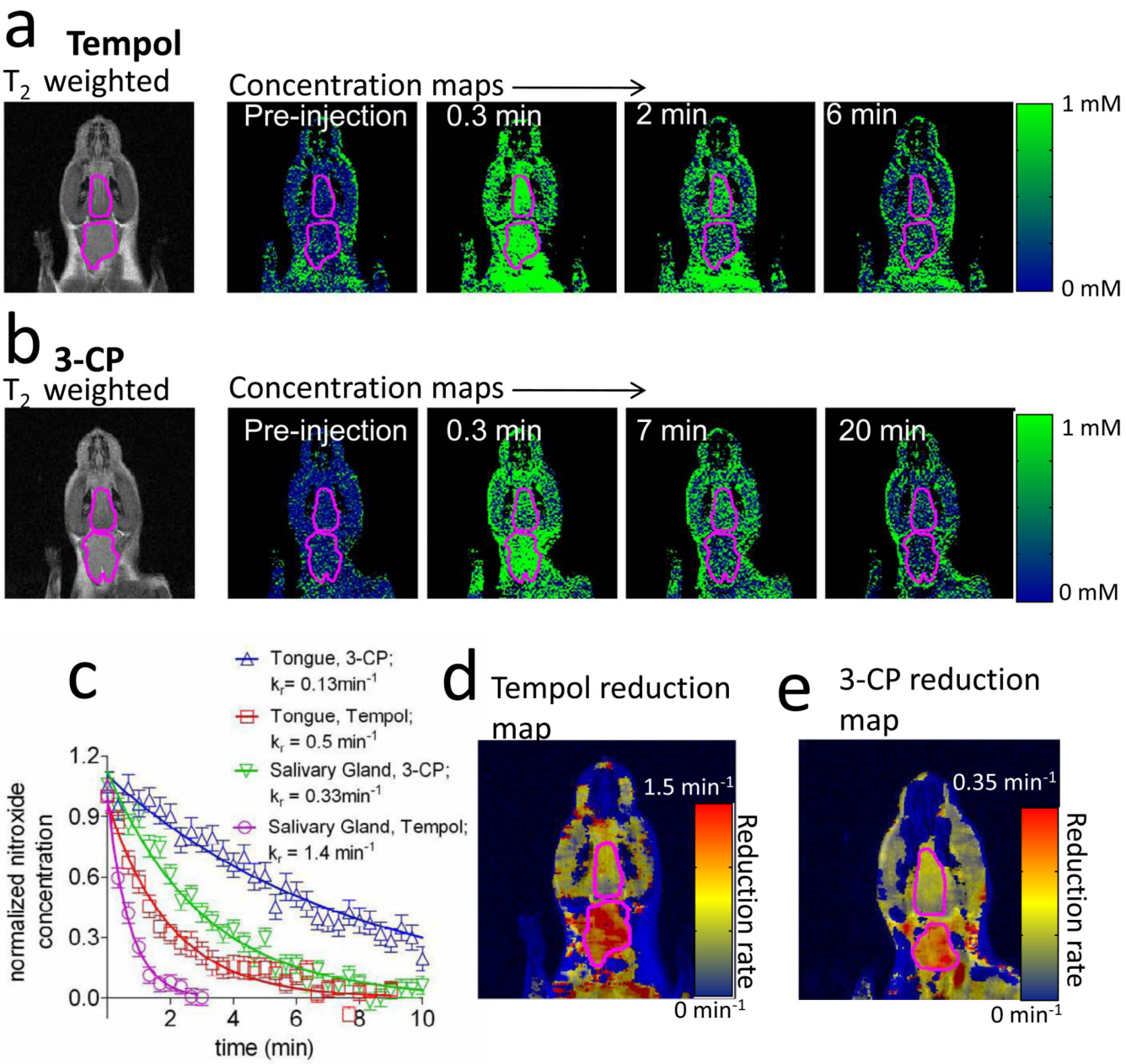

Figure 2.

Representative datasets showing Tempol and 3-CP reduction. a) An initial T_2 weighted image, followed by maps of Tempol concentration as a function of time after injection. The tongue (upper) and submandibular salivary gland (lower) ROIs are outlined in magenta. b) Same as "a", but with the nitroxide 3-CP instead of Tempol. c) Nitroxide concentration time-plots for the images in part "a." The concentration curves are normalized to the maximum observed concentration. d) Entire imaging timecourse compressed into a single image: a voxel by voxel reduction map of Tempol. Before computing the reduction maps, the concentration maps were spatially smoothed by an 11×11×1 voxel (1.7×1.7×1mm) averaging filter. e) Voxel by voxel reduction map of 3-CP.

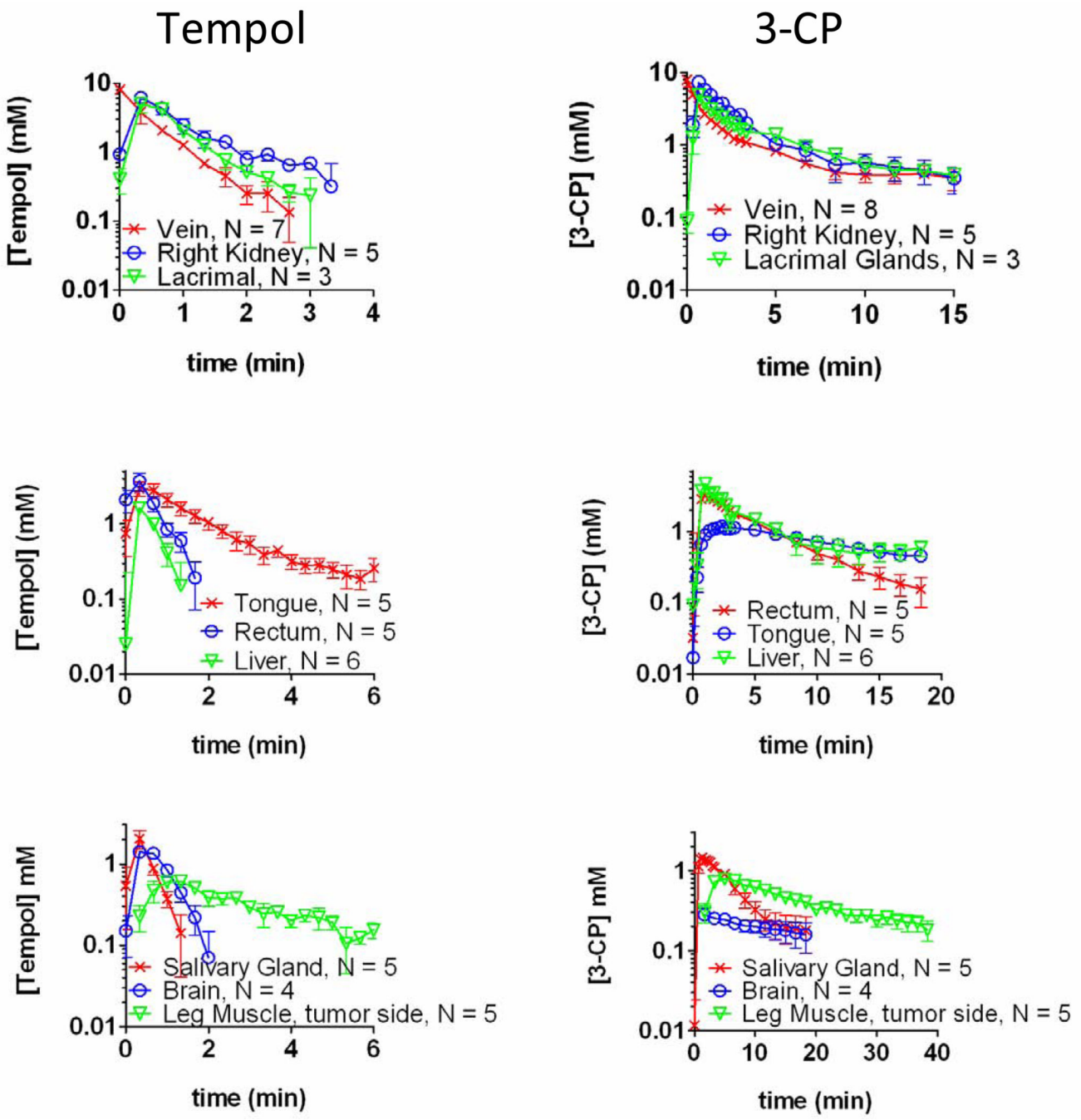

Figure 3.
Time-concentration curves of Tempol (a) and 3-CP (b) in various tissues. Error bars are the standard error of the mean concentration observed in all mice at a given time after injection.

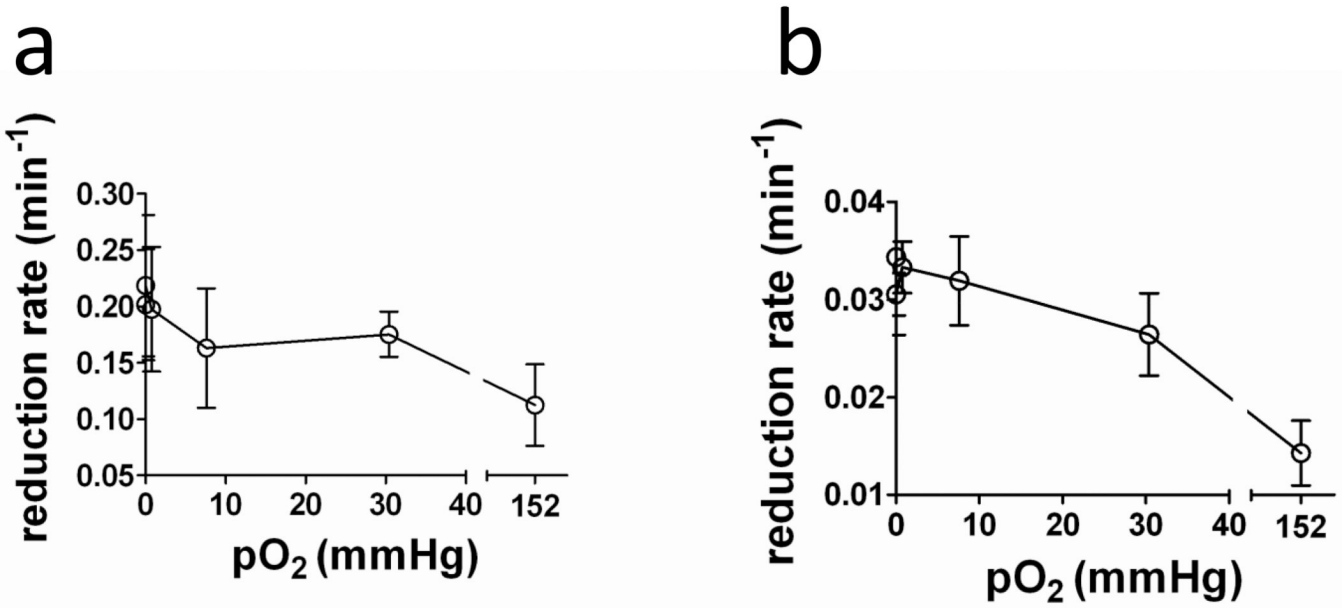

Figure 4.
Dependence of Tempol and 3-CP reduction on oxygen concentration. Error bars are the standard error of the mean of three measurements.

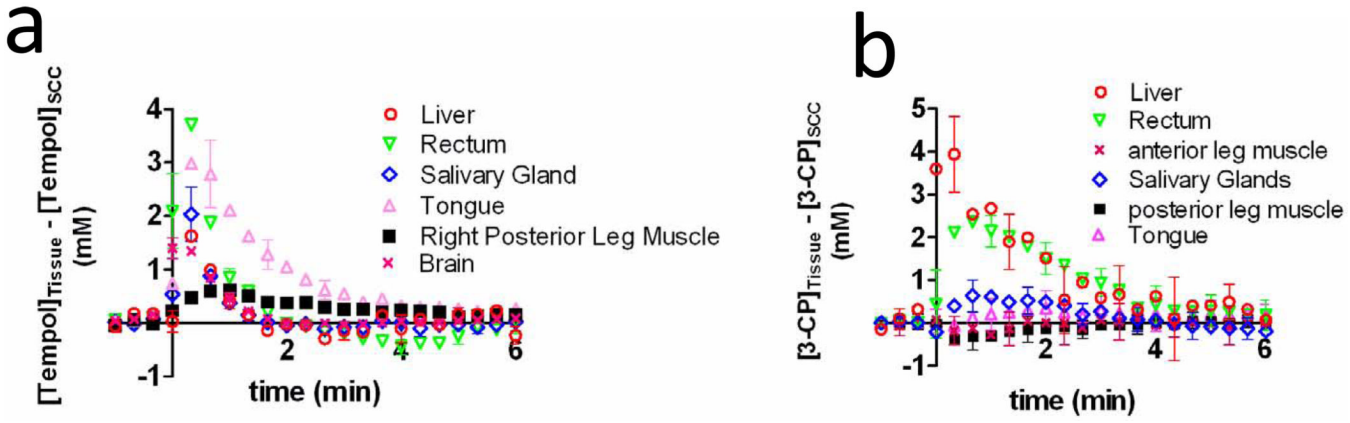

Figure 5.

Differential nitroxide concentration in various tissues. At each time-point, the concentration of nitroxide in SCC was subtracted from the concentration of nitroxide in each healthy tissues. Error bars are the propagated SEM of the difference.

Table 1

Reduction rates of Tempol and 3-CP in various tissues.

	3-CP					Tempol				
Tissue	**k_R**	**95% CI**	**N**	**P(≠JV)***	**P(≠LP musc)**	**k_R**	**95% CI**	**N**	**P(≠JV)**	**P(≠LP musc)**
Jugular Vein(JV) (1st phase)†	2.2	0.2	5	-	P <0.0001	2.2	0.2	7	-	P = 0.004
JV, (2nd phase)	0.33	0.04		-	-	-	-		-	
Lac Gland (LG) (1st phase)	1.9	0.4	5	P = 0.18	P <0.0001	2.1	0.3	3	P = 0.47	P < 0.0001
LG (2nd phase)	0.29	0.03		P = 0.11	-	-	-		-	
R Kidney(RK) (1st phase)	1.1	0.6	7	P = 0.055	P <0.0001	1.7	0.2	5	P = 0.002	P = 0.004
RK (2nd phase)	0.30	0.14		P = 0.81	-	-	-		-	
Liver	0.49	0.07	6	P < 0.0001	P <0.0001	1.6	0.5	5	P = 0.08	P = 0.003
Salivary Glands	0.22	0.03	8	P <0.0001	P <0.0001	2.3	0.15	5	P = 0.54	P < 0.0001
Brain	-	-		-	-	1.5	0.3	5	P = 0.078	P < 0.0001
Rectum	0.29	0.02	5	P <0.0001	P <0.0001	1.8	0.3	5	P = 0.11	P < 0.0001
Root of Tongue	0.10	0.02	5	P <0.0001	P <0.0034	0.86	0.08	5	P <0.0001	P = 0.024
LP muscle (contra to tumor)	0.06	0.03	5	P <0.0001	-	0.51	0.35	6	P = 0.046	P = 0.79
RP muscle (adjacent to tumor)	0.038	0.035	5	P <0.0001	P = 0.45	0.56	0.2	6	P = 0.004	-

*In the case of 3-CP, the jugular vein (JV), the lacrimal gland (LG), and the right kidney RK) exhibited a bi-exponential time-concentration curve (Figure 3). The reported P value for these tissues compares each exponential separately between data sets. For all other tissue P values, the JV was fit with a mono-exponential for the purpose of comparison.

†The "reduction rate" for the jugular vein reflects the rate at which the nitroxide is cleared (not reduced) from the blood pool.

Table 2

Tissues inaccessible to redox imaging

Tissue	Reason
Adipose tissue	no enhancement
Bone marrow	sub-resolution
Retina	no enhancement
Intestines	motion/motion artifacts (breathing)
Gallbladder	motion artifacts (breathing)/insufficient enhancement
Lungs	no T_1 weighted signal
Spleen	motion artifacts (breathing)

Table 3

In vivo reduction Rates of Tempol and 3-CP in various tumors

Tempol					
Tissue	**k_R**	**95% CI**	**N**	**$P(k_{R,tissue} \neq k_{R,SCC})$**	**$P(k_{R,tissue} \neq k_{R,muscle})$**
HT-29	0.64 m^{-1}	0.2 m^{-1}	4	**P < 0.0001**	P = 0.7014
KHT	0.91 m^{-1}	0.1 m^{-1}	4	**P = 0.002**	**P = 0.02**
SCC	1.2 m^{-1}	0.1 m^{-1}	5	-	**P = 0.0004**
3-CP					
SCC	0.11	0.01	6	-	**P = 0.0002**

Reported k_r are from a mono-exponential model.

Table 4

Maximum concentrations of Tempol and 3-CP in various tissues

	3-CP				Tempol				Two Tailed T-test
Tissue	**$[3\text{-CP}]_{max}$**	**SEM**	**t_{max}**	**N**	**$[Tpl]_{max}$**	**SEM**	**t_{max}**	**N**	**$P([3\text{-CP}]_{max} \neq [Tempol]_{max})$**
Jugular Vein	6.6 mM	2 mM	0 s	8	8.1 mM	1.3 mM	0 s	7	P = 0.54
SCC	0.9 mM	0.1 mM	160 s	6	0.8 mM	0.1 mM	0 s	5	P = 0.50
HT-29	-	-	-	-	0.6 mM	0.1 mM	20 s	4	-
KHT	-	-	-	-	0.6 mM	0.1 mM	40 s	4	-
Leg muscle (tumor side)	0.8 mM	0.1 mM	280 s	6	0.6 mM	0.1 mM	60 s	5	P = 0.20
Leg muscle (contra to tumor)	0.9 mM	0.1 mM	280 s	5	0.5 mM	0.1 mM	80 s	6	**P = 0.02**
Ant. leg muscle	0.9 mM	0.2 mM	220 s	5	1.1 mM	0.2 mM	40 s	6	P = 0.50
Brain	0.5 mM	0.1 mM	20 s	5	1.4 mM	0.2 mM	20 s	4	**P = 0.02**
Lacrimal glands	4.9 mM	0.5 mM	20 s	4	5.6 mM	0.8 mM	20 s	3	P = 0.51
Salivary Gland	1.4 mM	0.1 mM	60 s	7	2.0 mM	0.5 mM	20 s	5	P = 0.30
Rectum	3.1 mM	0.2 mM	40 s	5	3.7 mM	1 mM	20 s	5	P = 0.59
Root of Tongue	1.2 mM	0.4 mM	120 s	5	3.0 mM	0.6 mM	20 s	5	**P = 0.05**
Kidney (Left)	7.1 mM	0.5 mM	20 s	6	4.5 mM	0.7 mM	20 s	5	**P = 0.02**
Kidney (Right)	7.2 mM	0.5 mM	20 s	6	6.1 mM	0.8 mM	20 s	5	P = 0.29
Liver	4.7 mM	0.3 mM	20 s	6	1.6 mM	0.2 mM	20 s	6	**P < 0.01**

Significant P values are bold.

Table 5

Fractional Confidence Intervals for Reduction Rates

Tissue	3-CP	Tempol
Leg Muscle	**0.78**	1.3
SCC	**0.16**	0.46
Rectum	**0.29**	0.34
Liver	**0.67**	2.2
Salivary Gland	**0.22**	0.52
Kidney	**0.32**	0.54
Tongue	0.44	**0.15**

The 95% confidence interval and the reduction rate were calculated for each animal individually, and then averaged over all animals. Reported values are average confidence interval divided by the average reduction rate. For each tissue, the smaller confidence interval is in bold.